Journal of Sound and Vibration (1997) **208**(1), 55–71

VIBRATIONS OF SUBMERGED STRUCTURES IN A HEAVY ACOUSTIC MEDIUM USING RADIATION MODES

P.-T. CHEN

Department of Naval Architecture, National Taiwan Ocean University, Keelung 20024, *Taiwan, Republic of China*

(*Received* 27 *May* 1996, *and in final form* 19 *June* 1997)

A set of radiation modes developed in previous work (Chen and Ginsberg [1]) is further applied to the study of interactions between a heavy acoustic loading and an elastic structure. The coupling of the acoustic loading with the structure is carried out by using the radiation modes to decouple surface quantities into modal components together with a condensation of the structural equation onto the normal displacement of the wetted surface. Transforming the equation variables into velocity modal co-ordinates yields the equation for the submerged structure of which the unknown variable is the set of radiation modal amplitudes. The formulation provides a direct connection of the system response to the radiation modes, which characterizes acoustic behavior both at the surface and far fields. The radiation modes are divided into strong radiators and weak radiators, based on their magnitudes of the eigenvalues associated with the modal representation. Additionally, the interaction mechanism of the modes having strong radiation with the modes having weak radiation is presented in the formulation and demonstrated by numerical examples. The radiation patterns due to strong radiation modes exhibit directional characteristics, where the modal pressure distributions at the far field are confined to specific directions in space. Numerical examples are provided by beginning with a submerged constant thickness shell studied previously. The subsequent example is the shell attached with concentrated masses at various locations in order to reflect the changing of surface acoustic response and the far field response in terms of alterations to the structure.

INTRODUCTION

The interaction of a heavy acoustic medium with submerged elastic structures has been investigated extensively in recent decades. A conventional approach to describe the effect of acoustic loadings for surface acoustic quantities is by boundary integral equations or their alternative forms. Coupling the acoustic equation with the elastic structures yields the dynamic response of the coupled system under mono-frequency external excitations. This approach provides preliminary computational results, e.g., surface pressure, surface normal velocity, and displacement fields of the structures. However, the approach provides little information regarding acoustic radiation connected with the vibrational properties of the structures.

Recently, modal representations were established to disclose the surface normal velocity in connection with far field pressure. Borgiotti [2] and Photiadis [3] applied singular value decomposition to radiation operators which related the surface normal velocity to far field pressure to decouple the surface velocity into modal forms. Sarkissian [4] applied singular value decomposition to a surface impedance to derive radiation modes where the impedance is transformed to a symmetric matrix by multiplying a proper scaling shape

0022–460X/97/460055 + 17 $25.00/0/sv971193

factor. Cunefare [5] computed the radiated power in the far field from which the radiation modes were derived. The corresponding eigenvalues are proportional to the radiation efficiencies of the modes. Thus, the normal velocity on the surface can be factorized into each individual modal component such that each mode possesses its own radiation efficiency. Moreover, the velocity radiation modes can be essentially divided into either strong radiators, which radiate acoustic energies to the far field, or weak radiators, which respond primarily evanescent fields near the surface. This modal description has been applied to near field acoustic holography [2–4], optimization acoustic design [5–7], and noise control [8, 9]. The significant feature of such modal representations is parallel to vibrational modes in the area of structural dynamics. Therefore, expanding the above developments to include submerged elastic structures is significant to engineering applications. However, the acoustic mode stated above originates from the radiated acoustic power from vibrating surfaces as a function of surface velocity, bypassing the surface interaction mechanism between surface pressure and normal velocity. Also, the corresponding surface pressure of each modal velocity does not possess an orthogonal property which subsequently leads to difficulty in decoupling the surface pressure.

Since the coupling of an acoustic medium with elastic structures occurs on the surface in which both the pressure and velocity are generally involved in the formulation, a modal description that holds for both surface quantities is essential for a modal-type formulation. Such a requirement can be satisfied by using another form of modal representation, which is termed as acoustic pressure and velocity radiation modes, as established by Chen and Ginsberg [1]. The analysis, based on a perspective different from the previous ones, is derived from a complex surface acoustic power. The analysis starts by identifying an acoustic reciprocity for two various sets of surface pressures and normal velocities, subsequently leading to symmetric coefficients for the complex surface acoustic power. Two sets of symmetric eigenvalue problems arise when the complex surface power is diagonalized based on the discretized variables either by surface pressure or normal velocity. The eigensolutions of the two eigenvalue problems form a one-to-one correspondence of the pressure radiation modes and velocity radiation modes. The eigenvalues derived from each eigenvalue problem are shown to be identical and are identified as acoustic modal radiated powers for the modes whose magnitudes are normalized by unit reactive powers. In addition, these eigenvalues are related to the responding phases between pairs of pressure and velocity modes such that a large eigenvalue denotes a small phase and a small eigenvalue presents a phase close to 90°. Chen and Ginsberg also concluded that the set of the radiation modes can be divided into either strong radiators or weak radiators, based on the magnitudes of the eigenvalues such that a nearly zero eigenvalue is regarded as an inefficient radiator of that mode. One of the major differences of the modal representation by Chen and Ginsberg from the previous derivations [2–5] is that the acoustic radiation mode is derived for both surface pressure and velocity. The radiation mode derived by Chen and Ginsberg is used as the foundation of the present study.

In this study, the coupling of a heavy acoustic medium with elastic structures under a mono-frequency vibration is formulated by the radiation modes. The primary feature of the formulation is to present submerged structural responses in terms of acoustic radiation characteristics. The coupled system is formulated in terms of acoustic modal co-ordinates in which the structural equation is condensed onto the normal direction of the wetted surface with which inertia effects are included. The structure could have internal structural members. Numerical examples presented are a slender immersed spheroidal thin shell studied previously [10] as well as attachments of concentrated masses to the shell in order

to demonstrate variations of acoustic responses due to alterations of structural members. Also, the radiation patterns for the radiation modes are presented and discussed.

1. RADIATION MODES BASED ON A COMPLEX SURFACE ACOUSTIC POWER

The radiation mode [1] is first summarized based on a complex surface power. The surface pressure p and normal velocity v under an oscillation frequency ω can be superimposed by radiation pressure modes Ψ_j and radiation velocity modes Φ_j, respectively,

$$p = \sum_j P_j \Psi_j, \qquad v = \sum_j V_j \Phi_j, \tag{1}$$

where P_j and V_j are pressure and velocity modal amplitudes respectively. The orthogonal condition associated with Φ_j and Ψ_j is

$$\int_S \Psi_1 \Phi_m \, \mathrm{d}S = \delta_{1m} \sqrt{\lambda_m^2 + 1}, \tag{2}$$

where the surface integral is over the wetted surface of the structure. The subscripts 1 and m denote various modal states, and λ_m is the eigenvalue. Applying the above condition relates the modal amplitudes P_j and V_j to the surface pressure and velocity as

$$P_j = \int_S p\Phi_j \, \mathrm{d}S/\sqrt{\lambda_j^2 + 1}, \qquad V_j = \int_S v\Psi_j \, \mathrm{d}S/\sqrt{\lambda_j^2 + 1}. \tag{3}$$

Moreover, the amplitudes P_j and V_j are related by

$$P_j = V_j \, \mathrm{e}^{-\mathrm{i}\theta_j}, \tag{4}$$

where i denotes $\sqrt{-1}$, and the phase θ_j is defined by the eigenvalue λ_j such that

$$\theta_j = \tan^{-1} 1/\lambda_j. \tag{5}$$

Equations (4) and (5) indicate that the response of surface pressure due to a velocity distribution whose profile conforms to a velocity mode Φ_j is the corresponding pressure mode Ψ_j with a phase shift θ_j, and vice versa for the response caused by a pressure mode. Equations (1–5) constitute the modal description for acoustic responses on the surface. The dynamical characteristics are fully characterized by the acoustic modes Φ_j, Ψ_j and the eigenvalues λ_j such that every mode reacts independently. The surface complex acoustic power $\tilde{\mathbf{P}}$, defined as one half of the surface integral of the pressure product of the complex conjugate of velocity, can be expressed as a modal superposition, i.e.,

$$\tilde{P} = \frac{1}{2} \int_S pv^* \, \mathrm{d}S = \frac{1}{2} \sum_j |P_j|^2 (\boldsymbol{\lambda}_j - i) = \frac{1}{2} \sum_j |V_j|^2 (\boldsymbol{\lambda}_j - i). \tag{6}$$

The negative sign for the reactive power in equation (6) is intentionally used since the phase of surface pressure leads the normal velocity due to the fact that the surface acoustics is subject to fluid inertia and radiation damping. Here, the oscillation time factor is $\mathrm{e}^{-\mathrm{i}\omega t}$. The derivation of equation (6) has applied the orthogonality of equation (2). The equation indicates that the contribution of the radiated acoustic power from the jth radiation mode

is quantified by the value λ_j, and that a mode becomes a weak radiator when its eigenvalue approaches zero.

2. SUBMERGED STRUCTURAL RESPONSES USING ACOUSTIC RADIATION MODES

The formulation representing a submerged structure under a heavy acoustic medium loading and external exciting forces can be written as

$$\begin{bmatrix} M_{nn} & M_{ni} \\ M_{in} & M_{ii} \end{bmatrix} \begin{Bmatrix} \ddot{x}_n \\ \ddot{x}_i \end{Bmatrix} + \begin{bmatrix} K_{nn} & K_{ni} \\ K_{in} & K_{ii} \end{bmatrix} \begin{Bmatrix} x_n \\ x_i \end{Bmatrix} = \begin{Bmatrix} -\mathbf{N}^{\mathrm{T}}\{\mathbf{P}\} \\ 0 \end{Bmatrix} + \begin{Bmatrix} f_n \\ f_i \end{Bmatrix}, \tag{7}$$

where the discretization of the structure is made such that x_n denotes nodal values or assumed mode expansion coefficients for the normal displacement on the wetted surface, x_i is the displacement tangent to the surface as well as the degrees of freedom of internal structures, f_n and f_i are the applied forces corresponding to x_n and x_i respectively, and $\{\mathbf{P}\}$ is the pressure modal amplitude expanded by the radiation modes according to equation (1). The term $-\mathbf{N}^{\mathrm{T}}\{\mathbf{P}\}$ denotes the acoustic loading where $\mathbf{N}$ is a shape factor matrix having arisen from the discretization functions when one applies a virtual work done by the surface pressure to the normal displacement, that is,

$$\begin{aligned} \delta W_p &= -\int_S \left(\sum_j P_j \, \Psi_j \right) \delta \left(\sum_k x_{n,k} \, \phi_k \right) \mathrm{d}S \\ &= -\sum_j \sum_k P_j \, \delta x_{n,k} \int\int \Psi_j \, \phi_k \, \mathrm{d}S = -\sum_j \sum_k P_j \, \delta x_{n,k} \, N_{jk}, \end{aligned} \tag{8}$$

where ϕ_k is the discretization function on the normal direction of the wetted surface whose expansion coefficient or nodal value is $\mathbf{x}_{n,k}$, and δ denotes the virtual increment. The N_{jk} is identified as

$$N_{jk} = \int_S \Psi_j \, \phi_k \, \mathrm{d}S. \tag{9}$$

Equation (7) is then condensed to the normal direction $\mathbf{x}_n$ which can be done by using the second sub-matrices equation in equation (7) to express x_i as a function of x_n and f_i under a mono-frequency oscillation at frequency ω,

$$\{\mathbf{x}_i\} = (K_{ii} - \omega^2 M_{ii})^{-1} [f_i - (K_{in} - \omega^2 M_{in}) \{\mathbf{x}_n\}]. \tag{10}$$

Equation (10) states that once the displacement $\mathbf{x}_n$ is known, the tangential and interior displacements are determined accordingly by $\mathbf{x}_n$ and f_i. Substituting equation (10) into equation (7) yields the equation for $\mathbf{x}_n$ in terms of the external forces and pressure modal amplitudes,

$$\begin{aligned} &[(K_{nn} - \omega^2 M_{nn}) - (K_{ni} - \omega^2 M_{ni}) (K_{ii} - \omega^2 M_{ii})^{-1} (K_{in} - \omega^2 M_{in})] \{\mathbf{x}_n\} \\ &\quad = -\mathbf{N}^{\mathrm{T}}\{\mathbf{P}\} - (K_{ni} - \omega^2 M_{ni}) (K_{ii} - \omega^2 M_{ii})^{-1} f_i + f_n. \end{aligned} \tag{11}$$

The response can be expressed in terms of the radiation modes by further utilizing equations (1) and (4) to relate pressure modal amplitudes $\{\mathbf{P}\}$ and the normal displacement

to the velocity modal amplitudes. Since the surface normal displacement can be expanded, either based on the velocity radiation modes or the discretization functions ϕ_k, one has

$$\sum_k x_{n,k}\,\phi_k = \sum_m q_m\,\Phi_m = \sum_m q_m \sum_k\; T_{km}\,\phi_k = \sum_k \sum_m T_{km}\,q_m\,\phi_k,$$

which leads to the transformation

$$x_{n,k} = \sum_m T_{km}\,q_m,$$

or in matrix notation,

$$\{\mathbf{x}_n\} = [\mathbf{T}]\{\mathbf{q}\}, \tag{12}$$

where T_{km} is the expansion coefficients for the velocity mode Φ_m in terms of the discretization functions ϕ_k, and q_m is the normal displacement modal amplitude, which is related to V_m by

$$V_m = -\mathrm{i}\omega q_m. \tag{13}$$

Substituting equation (12) into equation (11) and premultiplying equation (11) by $\mathbf{T}^{\mathrm{T}}$ leads to

$$\mathbf{T}^{\mathrm{T}}\hat{\mathbf{K}}_{nn}\,\mathbf{T}\{\mathbf{q}\}_j = -\mathbf{T}^{\mathrm{T}}\mathbf{N}^{\mathrm{T}}\{\mathbf{P}\} + \mathbf{T}^{\mathrm{T}}\hat{f}_n, \tag{14}$$

where the matrix $\hat{\mathbf{K}}$ and equivalent normal force $\hat{f}_n$ are defined as

$$\hat{\mathbf{K}} = (K_{nn} - \omega^2 M_{nn}) - (K_{ni} - \omega^2 M_{ni})\,(K_{ii} - \omega^2 M_{ii})^{-1}(K_{in} - \omega^2 M_{in}),$$
$$\hat{f}_n = -(K_{ni} - \omega^2 M_{ni})\,(K_{ii} - \omega^2 M_{ii})^{-1} f_i + f_n. \tag{15}$$

The first term on the right side of equation (14) can be further derived by applying equations (2), (4), (9), (12), and (13), so that

$$\mathbf{T}^{\mathrm{T}}\mathbf{N}^{\mathrm{T}}\{\mathbf{P}\} = \sum_m \sum_j T_{jk}\,N_{mj}\,P_m = \sum_m \sum_j T_{jk}\left(\int_S \Psi_m\,\phi_j\,\mathrm{d}S\right)P_m = \sum_m \int_S \Psi_m\left(\sum_j T_{jk}\,\phi_j\right)\mathrm{d}S P_m$$

$$= \sum_m \left(\int_S \Psi_m\,\Phi_k\,\mathrm{d}S\right)P_m = \sum_m \delta_{mk}\sqrt{\lambda_k^2 + 1}\,P_m$$

$$= \sum_m \delta_{mk}\sqrt{\lambda_k^2 + 1}(-\mathrm{i}\omega)\,\mathrm{e}^{-\mathrm{i}\theta_m} q_m = \sum_m \delta_{mk}\,(\boldsymbol{\lambda}_k - i)\,(-\mathrm{i}\omega) q_m, \tag{16}$$

where the symbol δ_{mk} denotes the Kronecker delta symbol indicating that the associated terms form a diagonal matrix. Thus, equation (14) becomes

$$[\mathbf{T}^{\mathrm{T}}\hat{\mathbf{K}}\mathbf{T}]\{\mathbf{q}\} + [\delta_{mk}\,(\boldsymbol{\lambda}_k - \mathbf{i})\,(-\mathrm{i}\omega)]\{\mathbf{q}\} = \mathbf{T}^{\mathrm{T}}\hat{f}_n, \tag{17}$$

which is the governing equation for the submerged structure using the radiation modal amplitudes $\{\mathbf{q}\}$ as variables. The first term denotes the condensed dynamic stiffness in the situation of the constant oscillation frequency ω using velocity radiation modes as modal co-ordinates, and the second diagonal term denotes the acoustic loading due to the radiation modes. Recall equation (6) that the factor $(\lambda_k - i)$ represents the complex modal

power of a unit velocity modal amplitude. Thus, equation (17) shows that the acoustic loading due to the radiation modes is proportional to the corresponding complex modal powers. As expected from the physical phenomenon, the term associated with λ_k in equation (17) is an imaginary coefficient, which denotes damping effects to the structure. Meanwhile, the term associated with the reactive power provides restoring effects, which do not dissipate energy. A comparison of the sign of the mass effects in the structural equation shows that the negative reactive power term indicates inertia effects to the structure.

3. COUPLING OF STRONG AND WEAK ACOUSTIC RADIATION MODES FOR SUBMERGED ELASTIC STRUCTURES

Equation (17) provides a further insight into the interactions between strong radiation modes and weak radiation modes in relation to the structural properties. This interaction becomes clear when equation (17) is partitioned on the basis of the modal attributes of efficient and inefficient radiators,

$$\begin{bmatrix} \mathbf{T}_e^{\mathrm{T}}\,\hat{\mathbf{K}}\mathbf{T}_e + \delta_{km}\,(\boldsymbol{\lambda}_k - i)\,(-\mathrm{i}\omega) & \mathbf{T}_e^{\mathrm{T}}\,\hat{\mathbf{K}}\mathbf{T}_i \\ \mathbf{T}_i^{\mathrm{T}}\,\hat{\mathbf{K}}\mathbf{T}_e & \mathbf{T}_i^{\mathrm{T}}\,\hat{\mathbf{K}}\mathbf{T}_i + \delta_{km}\,(-\mathrm{i})\,(-\mathrm{i}\omega) \end{bmatrix} \begin{Bmatrix} q_e \\ q_i \end{Bmatrix} = \{\mathbf{T}^{\mathrm{T}}\hat{f}_n\}, \tag{18}$$

where q_e and q_i are the modal amplitudes for efficient and inefficient radiators, respectively, and the matrices $\mathbf{T}_e$ and $\mathbf{T}_i$ are the partitioned matrices of the transformation matrix $\mathbf{T}$ based on efficient or inefficient radiators. Here, the eigenvalues in the above equation associated with inefficient radiators have been set to zero. The equation indicates that the interactions for the modes of strong and weak radiators occur at the coupling stiffnesses $\mathbf{T}_e^{\mathrm{T}}\,\hat{\mathbf{K}}\mathbf{T}_i$ and $\mathbf{T}_i^{\mathrm{T}}\,\hat{\mathbf{K}}\mathbf{T}_e$. The influence of weak radiators $\{\mathbf{q}_i\}$ to strong radiators $\{\mathbf{q}_e\}$ depends on the coupling stiffnesses and external forces having the components of the inefficient radiation modes. A numerical example to demonstrate the coupling effect of the weakly radiating to strongly radiating modes will be provided later. Note that equation (17) is a symmetric formulation.

Once $\{\mathbf{q}_e\}$ and $\{\mathbf{q}_i\}$ are solved, surface responses are obtained by combining equations (1), (4), and (13), and the complex power is calculated using equation (6). The real part of the complex power is the radiated power. The normal displacement $\{\mathbf{x}_n\}$ of the structure follows the transformation of equation (12), while the corresponding $\{\mathbf{x}_i\}$ is computed by equation (10) accordingly. The field pressure at a field point $\mathbf{x}$ is obtained by equations (1), (4) and the Helmholtz integral formula

$$\begin{aligned} p(x) &= \int_S \left[p(y)\frac{\partial G(x,y)}{\partial n} - \rho_0\,\mathrm{i}\omega v_n\,(y) G(x,y) \right] \mathrm{d}S_y \\ &= \int_S \left[\left(\sum_j P_j\,\Psi_j\,(y) \right) \frac{\partial G(x,y)}{\partial n} - \rho_0\,\mathrm{i}\omega \left(\sum_j V_j\,\Phi_j\,(y) \right) G(x,y) \right] \mathrm{d}S_y \\ &= \int_S \left[\left(\sum_j V_j\,\mathrm{e}^{-\mathrm{i}\theta_j}\Psi_j\,(y) \right) \frac{\partial G(x,y)}{\partial n} - \rho_0\,\mathrm{i}\omega \left(\sum_j V_j\,\Phi_j\,(y) \right) G(x,y) \right] \mathrm{d}S_y \\ &= \sum_j V_j \int_S \left[\mathrm{e}^{-\mathrm{i}\theta_j}\Psi_j\,(y)\,\frac{\partial G(x,y)}{\partial n} - \rho_0\,\mathrm{i}\omega\Phi_j\,(y) G(x,y) \right] \mathrm{d}S_y, \end{aligned} \tag{19}$$

where G is a free space Green's function having a factor $1/(4\pi R)\exp(ikR)$, in which k is the wave number, $\partial G/\partial n$ is the normal derivative of G, ρ_0 is the fluid density, and y denotes the source point on the wetted surface. The integral of the last expression is identified as the field pressure caused by the jth acoustic mode of which the velocity is Φ_j and the pressure is $\Psi_j e^{-i\theta_j}$. Equation (19) is a modal-type representation for the field pressure response where V_j is related to the solved normal displacement modal amplitude q_j by equation (13).

The radiation pattern is obtained by allowing the point x in equation (19) to approach a large distance R and factoring out the simple source factor e^{-ikR}/R from the equation, where R is the distance of a point at the far field to a reference origin point of the body. Because the pressure waves due to the weak radiator modes are confined to the near-field of the surface, equation (19) can be simplified by only accounting the contributions of the strong radiation modes. The modal radiation patterns of the radiation modes are examined in the following.

4. RADIATION PATTERNS FOR RADIATION MODES

Radiation patterns for radiation modes were found first in literature [4] for which the modes were derived on the basis of singular value decomposition applied to the real part of the impedance of the surface acoustic loading. A finite rigid cylinder was used as an example to demonstrate that the patterns for strong radiator modes have directional or beaming characteristics, and that the patterns for weak radiator modes vanish in the far field. A cut-off wave number exists for a mode whose phase speed is equal to the sound speed of the acoustic medium. A sudden drop of radiation efficiencies, e.g., singular values, versus mode numbers was observed. A similar situation occurs with the radiation modes presently used. Figures 1 and 2 are the plots of pressure and velocity radiation modes for the first eight modes, which are copied from the previous study [1]. The arc length is non-dimensionalized by the total arc length between the two apexes of the spheroid. The geometry is a slender spheroidal body whose aspect ratio of major radius to minor radius is four under a non-dimensional oscillation frequency $ka = 1{\cdot}8$, where $k = \omega/C_0$, and C_0 is the sound speed. The quantities presented are non-dimensionalized by the minor radius a for spatial quantities, and by $\rho_0 C_0^2$ for pressure where ρ_0 is the fluid density. The corresponding eigenvalues λ_j are listed in Table 1. The radiation patterns are shown in Figures 3 and 4, which are computed by the integral of the last expression of equation (19). The orientations of 0° and 180° are along the apex directions, and 90° is normal to the direction of the surface around the equator. The patterns present directional features in which the far field pressures move from 90° toward 0° and 180° gradually when the mode numbers increase from the first to the sixth. Beyond the seventh mode, the patterns start to shrink to smaller values, whilst the corresponding eigenvalues abruptly drop to small values. A similar phenomenon has also been observed in the literature [4] for the case of a finite rigid cylinder.

These manifestations can be accounted for by the trace velocity matching principle [11]. The principle states that a supersonic wave travelling on a flat surface, whose speed C_w is greater than the sound speed C_0, generates acoustic waves into the acoustic medium. The propagating direction is the direction in which the phase velocity of the acoustic wave along the surface equals the supersonic wave speed. A subsonic wave, whose speed is less than the sound speed, produces an evanescent pressure field that does not radiate energy into the far field. Figure 5 shows the relationship between the supersonic wave speed C_w and the sound speed C_0. The matching principle, although valid only for flat surfaces, is still qualitatively applicable to a curved surface when the surfaces are relatively flat in

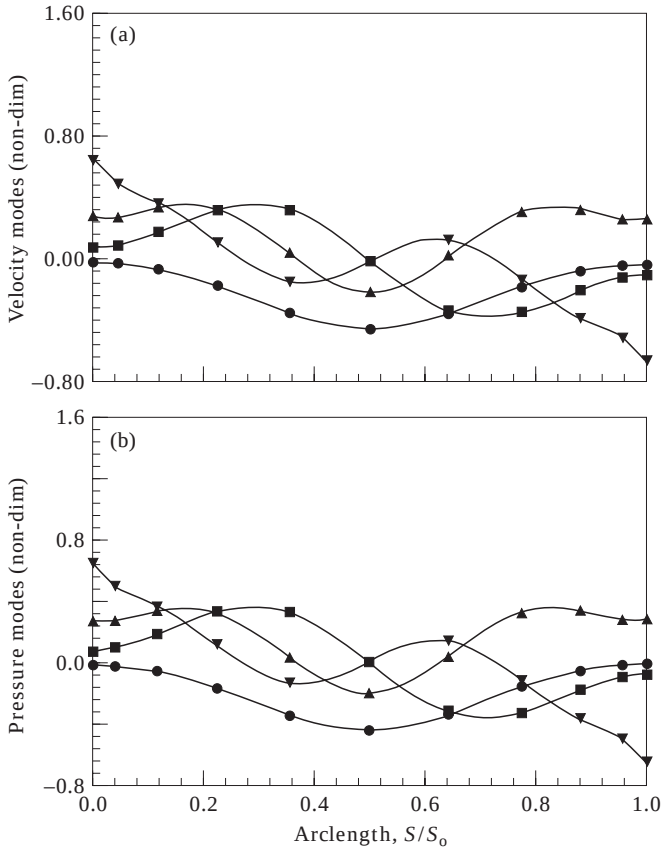

Figure 1. (a) Acoustic velocity and (b) pressure radiation modes for the first four modes at $ka = 1{\cdot}8$. Key: —●—, mode 1; —■—, mode 2; —▲—, mode 3; —▼—, mode 4.

some regions. The velocity profiles of the velocity modes depicted in Figures 1 and 2 can be decomposed into wave number components. The simple variations of the profiles denote that the wave number components are narrow bands. Each wave component is responsible for a principal radiation direction determined by the matching principle. The small wave number, which corresponds to a large travelling speed, generates propagating waves in a direction nearer perpendicular to the surface (see Figure 5). The large wave number, but still a supersonic wave, causes waves to propagate in a direction nearer to parallel with the surface. As the wave number further increases, the travelling speed on the surface is less than the sound speed which leads to the waves becoming evanescent so that the pressure decays rapidly from the surface. The sudden jump of the eigenvalues in Table 1 indicates the occurrence of a cut-off wave number that divides the velocity profiles of the modes into supersonic and subsonic waves. As a result of such directional features, the far field pressure essentially consists of contributions by a single or two strongly radiating modes, rather than the overall modes which radiate efficiently.

The coupled system equation of equation (17), the modal representation of surface quantities of equation (1), and field pressure superposed by the radiation modes of equation (19), constitute a modal-type formulation for acoustic–structural interactions. Numerical examples are provided in the next section.

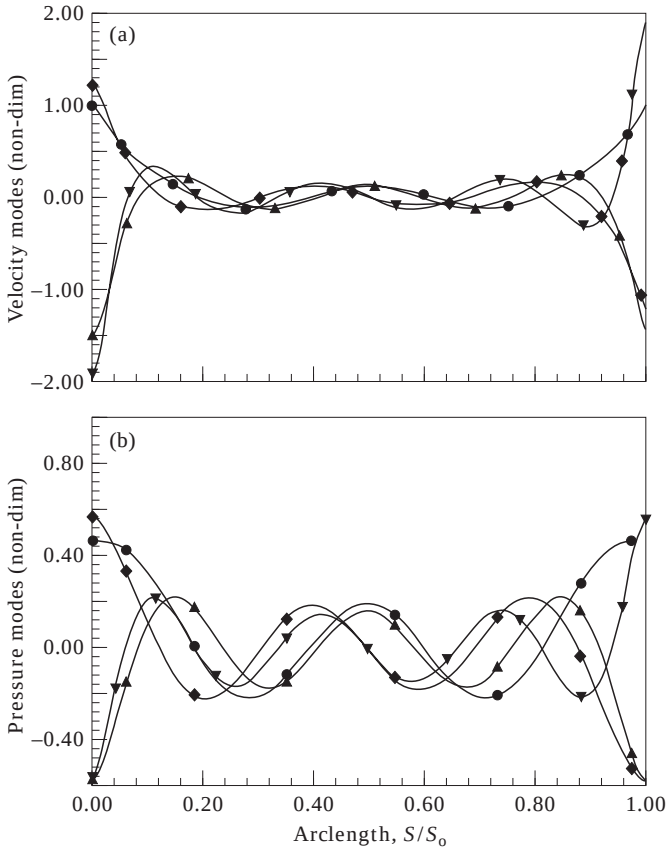

Figure 2. (a) Acoustic velocity and (b) pressure radiation modes for the fifth to eighth modes at $ka = 1{\cdot}8$. Key: —●—, mode 5; —■—, mode 6; —▲—, mode 7; —▼—, mode 8.

5. NUMERICAL EXAMPLES

The present formulation is demonstrated using a constant thickness spheroidal shell as a primary model [10], together with attachments of concentrated masses to the shell. The former is to illustrate the response of submerged elastic structures by the velocity modal co-ordinates. The latter addresses variations of acoustic field when the structural properties are varied. The parameters selected for the shell are identical with those in reference [10]: the ratio of dilatation wave speed of the shell's material to acoustic wave speed of the medium, $c_d/c_0 = 3{\cdot}367$, the density ratio between the shell and fluid, $\rho_s/\rho_0 = 7{\cdot}9$, the thickness ratio of the shell to the minor axis radius, $h/a = 0{\cdot}03$, and the non-dimensional exciting frequency $ka = 1{\cdot}8$.

The shell equation is based on classical linear bending thin shell theorems, formulated in axisymmetric response using Hamilton's principles in conjunction with a Raleigh–Ritz

TABLE 1

Eigenvalue λ_j for a prolate spheroid of an aspect ratio 4 *at* $ka = 1{\cdot}8$

Mode number	1	2	3	4	5	6	7	8
Eigenvalue	3·34	2·80	2·18	1·50	0·895	0·361	0·090	0·01390

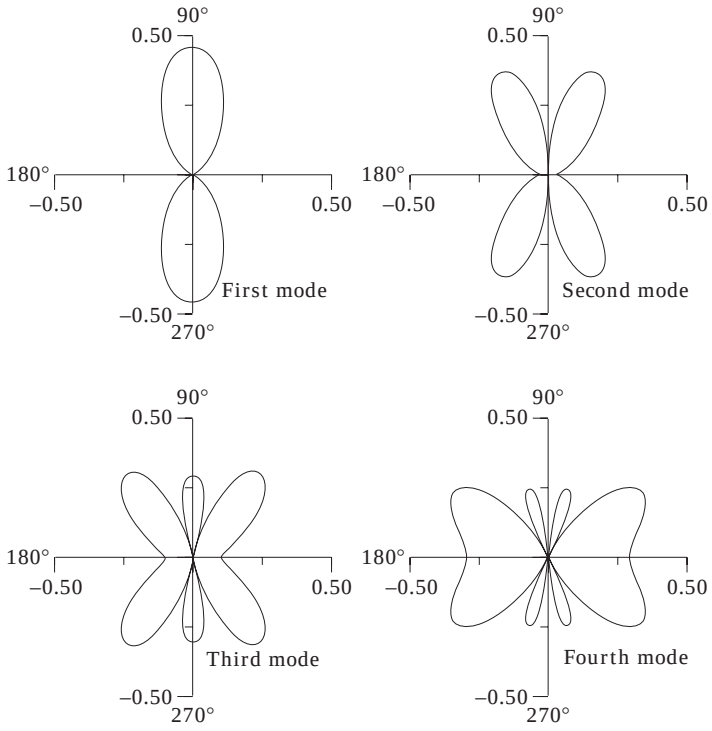

Figure 3. Radiation patterns due to the first four acoustic radiation modes.

type assumed modes expansion for the normal displacement and tangential displacement. The derivation can be found in references [10, 12]. Substituting the radiation modal modes into equation (17) yields the equation of the coupled system in terms of radiation modal amplitudes $\{\mathbf{q}_i\}$. The external force is a unit uniform surface force non-dimensionalized by a factor of $\rho_0 c_0^2$. The velocity modal amplitudes, which relate the displacement modal amplitudes by equation (13), are listed in the second column of Table 2 with the corresponding external modal forces $\hat{f}_i$ tabulated in the third column. The radiated power is simply summed up algebraically over each modal power computed by equation (6). The radiated powers due to the uniform surface force are listed in the fourth column. This table clearly shows that the response is attributed to the first radiation mode. Correspondingly, it is not surprising as displayed in Figure 6 that the far field pressure occupies the region in the directions of 90° and 270° as one realizes that the radiation pattern of the first mode is mainly distributed in that region.

As another example in contrast to the uniform force, the external force is replaced by a unit concentrated point force, non-dimensionalized by a factor $\rho_0 c_0^2 a^2$, exerted at the apex located at 0°. The results are listed in Table 2 in which some of the weakly radiating modes have significant amplitude values shown in the fifth column. The occurrence of such a situation is due to the high order modal force components for the point force listed in the sixth column. As expected, the radiation pattern for the point force depicted in Figure 6 indicates that the pressure distribution in the regions of 90° and 180° becomes much smaller, while it is enhanced in the direction along the point force. Although there are obvious amplitudes for modes above the sixth mode, these modes contribute very little to far fields because of their inefficient radiation. The present modal-type formulation provides a direct connection for the surface responses to acoustic radiation characteristics.

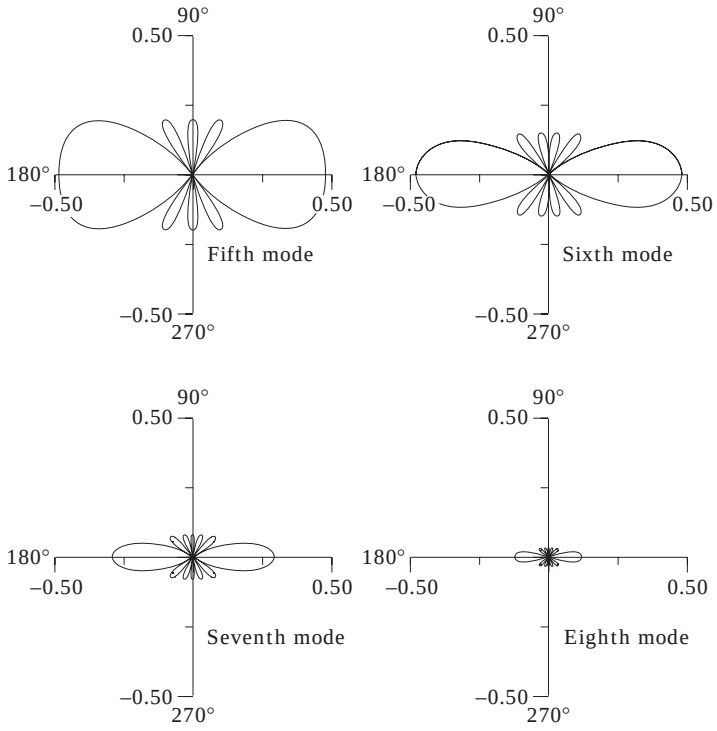

Figure 4. Radiation patterns due to the fifth to eighth acoustic radiation modes.

The amplitudes for the case of the point force do not approach zero for high order weak radiator modes, which is contrary to natural mode expansions in the area of structural dynamics. Such a situation will be interpreted in the next section.

The next example is a study of various concentrated masses attached to the shell under a uniform surface exciting force, in which the effects of structural alterations in relation to acoustic far fields are demonstrated. Two situations are calculated: a uniformly distributed line mass along the equator where the amount of mass is one-half of a spherical shell whose radius is the minor radius of the spheroidal shell with the identical thickness; two equal masses attached at the two apexes with each having one-half of the former added mass on the equator. The surface normal displacements, magnitudes of modal velocity amplitudes and far field radiation patterns are presented in Figures 7–9 respectively, where the results of the uniform thickness shell are included for comparison. Only symmetric modes whose profiles are symmetric about the equator are taken into account because the

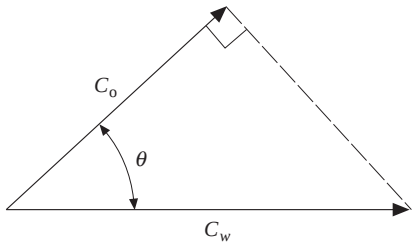

Figure 5. The relationship between supersonic wave speed C_w and sound speed C_0.

TABLE 2

Modal displacement amplitudes, modal forces, and radiated modal powers for a uniform surface force and a point force at $ka = 1{\cdot}8$

	Uniform surface force			Concentrated force		
Mode number	Velocity ampl.	Modal force	Modal radiated power	Velocity ampl.	Modal force	Modal radiated power
1	1·97352	−0·30395	6·45156	0·29417	−0·00148	0.14335
2	0·00000	0·00000	0·00000	0·34084	−0·00817	0·16217
3	0·44546	−0·16620	0·21635	0·62235	−0·03087	0·42229
4	0·00000	0·00000	0·00000	0·03415	−0·08139	0·00088
5	0·54108	−0·07790	0·13416	0·95363	−0·14477	0·41673
6	0·00000	0·00000	0·00000	0·75994	−0·20064	0·10375
7	0·55724	0·01629	0·01389	0·87306	0·23693	0·03409
8	0·00000	0·00000	0·00000	0·33841	−0·31911	0·00076
9	0·28540	−0·00122	0·00005	0·40978	0·22727	0·00010
10	0·00000	0·00000	0·00000	0·18037	−0·24410	0·00000
11	0·11926	0·00004	0·00000	0·17389	−0·31670	0·00000
12	0·00000	0·00000	0·00000	0·08648	−0·36066	0·00000
13	0·00000	0·00000	0·00000	0·04450	−0·00336	0·00000
14	0·00079	0·00000	0·00000	0·01211	0·22428	0·00000
15	0·00000	0·00000	0·00000	0·08945	−0·00489	0·00000
16	0·03152	0·00000	0·00000	0·06110	−0·15003	0.00000
17	0·02762	0·00000	0·00000	0·07258	0·14777	0·00000
18	0·00000	0·00000	0·00000	0·10256	−0·00486	0·00000
19	0·01059	0·00000	0·00000	0·11868	0·09733	0·00000
20	0·00000	0·00000	0·00000	0·23868	−1·52307	0·00000
21	0·05219	−0·00086	0·00000	0·16547	−1·65904	0·00001
Total radiated power	–	–	6·81601	–	–	1·28410

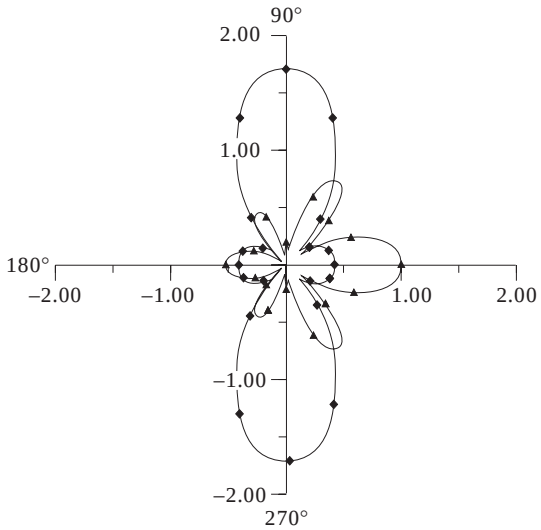

Figure 6. Radiation patterns of a constant thickness shell for a point and a uniform excitating forces at $ka = 1{\cdot}8$. Key: —▲—, point force; —◆—, uniform loading.

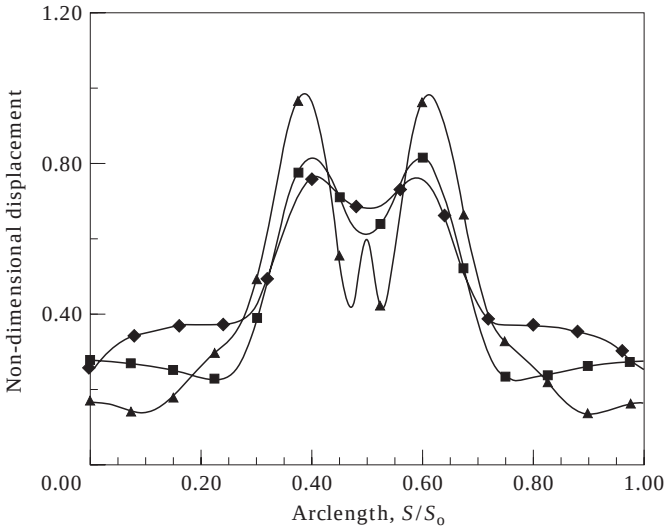

Figure 7. Surface displacements under a uniform exciting force for a constant thickness shell as well as with various attached masses at $ka = 1{\cdot}8$. Key: —◆—, uniform thickness; —■—, added masses at apexes; —▲—, added masses at equator.

responses are symmetric about the equator. Evaluating the radiation characteristics from the plots of surface responses, such as in Figure 7, is relatively difficult. However, the modal amplitudes plotted in Figure 8 clearly reveal radiation situations and their connections to radiation patterns. The modal amplitude distributions for the case of two concentrated

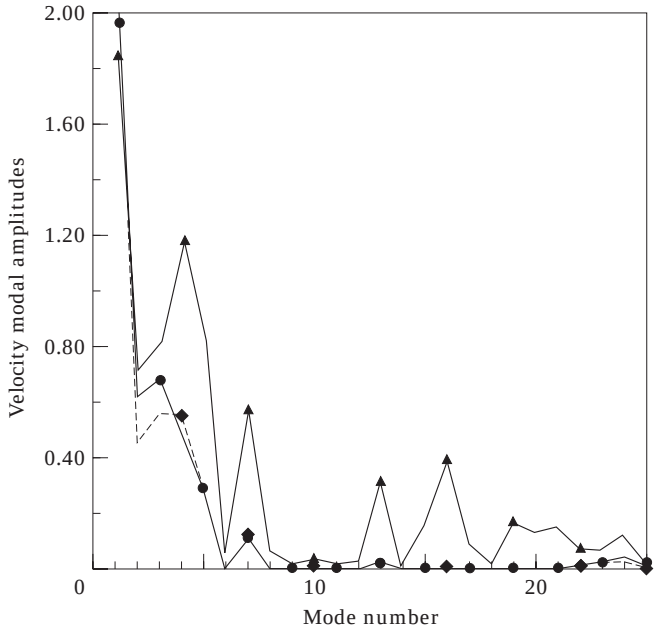

Figure 8. Modal velocity amplitudes under a uniform exciting force for a constant thickness shell as well as with various attached masses at $ka = 1{\cdot}8$. Key: —◆—, uniform thickness; —●—, added mass at apexes; —▲—, added mass at equator.

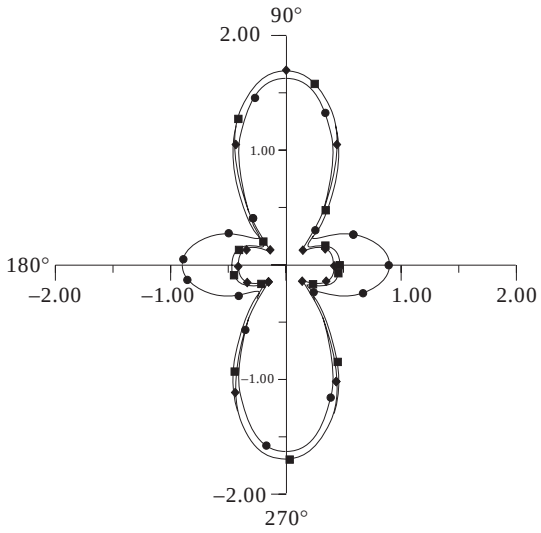

Figure 9. Radiation patterns under a uniform exciting force for a constant thickness shell as well as various attached masses at $ka = 1{\cdot}8$. Key: —◆—, uniform thickness; —●—, added mass at apexes; —■—, added mass at equator.

masses at the apexes are essentially the same as the case of uniform thickness except there are minor differences at the second and third modes, which shows that the radiation patterns of these two are nearly identical. In contrast to the case of two concentrated masses, the case of mass equally distributed at the equator has more high order weak radiator modes excited. The presence of the second and third modal amplitudes (which are numbered as the third and fifth modes for full modal numbers) yields the occurrence of the relative larger side lobes on the axisymmetric axis direction. The modes beyond the third mode, although presenting obvious amplitudes, do not contribute to the side lobes because the associated eigenvalues are small as listed in Table 1.

The surface complex powers calculated from equation (6) for the uniform thickness, added mass on the equator, and two added masses at the apexes are $(6{\cdot}78 - i2{\cdot}36)$, $(6{\cdot}59 - i3{\cdot}66)$, and $(7{\cdot}07 - i2{\cdot}49)$, respectively. The increased amount of radiated energy for the case of two concentrated masses is due to the increased modal acoustic energies of the second and third modes. The decreased radiated energy for the distributed mass around the equator is the decreased power of the first mode and relatively small increased powers of the second and third modes. Recall from equation (17) that a reactive power represents inertia effects to the structures. If the uniform thickness shell is taken as a reference, the increased amplitudes of weakly radiating modes for the distributed mass attached at the equator induce more inertia effects to the structure, whereas the added masses on the apexes induce less inertia effects because the modal amplitudes of high order modes are essentially the same as the uniform shell.

6. CONVERGENCE OF MODAL AMPLITUDES

The convergence of modal amplitudes versus the number of employed radiation modes used is examined by plotting the modal amplitudes versus mode numbers. Figure 10 shows the modal amplitudes for the point force where values are only meaningful at discrete integer mode numbers. The plot shows that the amplitudes do not approach unique values

for some high order modes, nor do they approach zero. This phenomenon can be interpreted from the properties of eigensolutions when the eigenvalues remain close to each other. It has been shown in reference [13] that for the situation of two eigenvalues staying in close proximity, the eigenfunctions exhibit high sensitivity to a perturbation of the eigensystem. The analysis can be extended to a cluster of close eigenvalues qualitatively. A perturbed eigenfunction ϕ_i' can be represented by linear combinations of unperturbed eigenfunctions ϕ_j whose eigenvalues remain close to each other,

$$\phi_i' = \sum_{j=1}^{n} c_{ij}\,\phi_j + \mathcal{O}(\varepsilon), \qquad i = 1, 2, \ldots n, \tag{20}$$

where c_{ij} is the combination coefficient which is strongly dependent on the small perturbation quantity indicated by ε, n is the number of the eigenvalues staying in the cluster, $\mathcal{O}(\varepsilon)$ and is a small quantity representing the contributions due to eigenfunctions whose eigenvalues are well separated from the cluster. Here, the eigenfunctions ϕ_i' and ϕ_j are normalized with some scales, which can be a unit reactive power in the present case. Because the high order weak radiating modes have nearly zero eigenvalues, implying that the eigenvalues remain close to one another, the corresponding radiating modes follow equation (20) and have strong dependence on a small disturbance. The disturbance could be any small alterations, including numerical discretization and numerical truncation errors. Various numbers of modes used denote different small alternations which lead to various modal amplitudes for high order modes as depicted in Figure 10. Therefore, numerically determining an "exact" high order radiation mode is nearly impossible. However, this situation does not pose any difficulty in applications since a numerically computed high order mode is the linear combination of the "exact" modes whose eigenvalues are nearly zero. Thus, the numerically computed modes still carry the acoustic modal characteristics of inefficient radiation. Therefore, the convergence is assessed by the

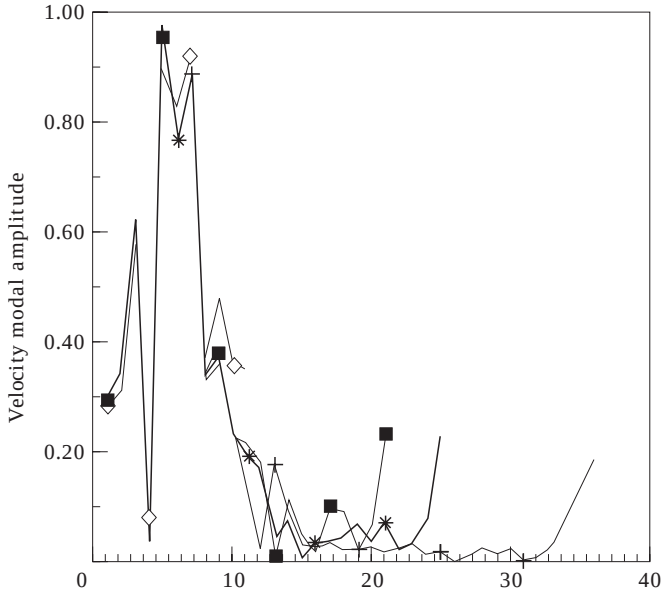

Figure 10. Velocity modal amplitudes of a constant thickness shell subject to a point force for various numbers of modes used at $ka = 1{\cdot}8$. Key: —◇—, 11 acoustic modes; —■—, 20 acoustic modes; —∗—, 25 acoustic modes; —+—, 35 acoustic modes.

convergence of the modal amplitudes whose eigenvalues are not zero, which are strong radiating modes and whose eigenvalues, although small, are not zero. In equation (18), the convergence of efficient radiator amplitudes $\{\mathbf{q}_e\}$ is achieved only when $\{\mathbf{q}_i\}$ has sufficient degrees of freedom to represent the structural responses, because $\{\mathbf{q}_e\}$ and $\{\mathbf{q}_i\}$ are coupled by the off-diagonal matrices. Moreover, the reactive power due to the weakly radiating modes is shown to converge when sufficient modes produce convergent results. Figure 10 shows that the use of 20, 25, and 35 modes yields converged answers, whereas 11 modes do not. The reactive power in Figure 10 contributed by the modes beyond the tenth mode are $-0{\cdot}11$, $-0{\cdot}10$, and $-0{\cdot}091$ for 20, 25, and 35 modes used, respectively. The example shows that 20 modes are sufficient for convergence in the case of the point force.

CONCLUSIONS

A formulation has been presented in this study for a heavy acoustic medium interacting with elastic structures using recently developed acoustic radiation modes. The representation of the structures is condensed to the degree of freedom on the normal direction of the wetted surface with inertia effects included under a mono-frequency oscillation. A coupled equation is derived by coupling the radiation modes to the condensed equation. Transforming the coupled equation into the radiation modal co-ordinates leads to the equation becoming an in-vacuo dynamic stiffness plus a diagonal term due to the acoustic loading. Each element of the diagonal terms has a one-to-one correspondence to surface complex modal powers for which the real part of the power represents the damping effects, and the imaginary part denotes inertia effects to the structure. The solved modal amplitudes of the equation lead to the surface response, structural displacements, and field pressures. The significant feature of the formulation is that the response of the coupled system is directly related to acoustic radiations through the acoustic radiation modes. A slender spheroidal body is used to show the modal radiation patterns such that the pressure at a far field position is mainly caused by a single or two modes emitted from the surface.

The present developments were demonstrated by using a submerged spheroidal shell with various attached masses under a point and uniform alternative forces. The case of a constant thickness shell under the uniform applying force was studied by using the present formulation, indicating that the first radiation mode was the primary one for the system response. A correlation was also studied between modal amplitudes and directivity of radiation patterns. In addition, the case of a point force acting on one apex, in contrast to the uniform force, was presented to display the excitation of weak radiator modes. Also, the convergence of the modal amplitudes versus numbers of modes was examined. Numerical results showed that the amplitudes of strongly radiating modes and low order weakly radiating modes converged when sufficient modes were used. Meanwhile, the amplitudes of high order modes, whose eigenvalues are nearly zero, did not approach finite values, nor null values. This numerical phenomenon is due to the nature of eigensolutions when the eigenvalues become close to one another such that the eigenfunctions are highly dependent on tiny perturbations applied to the eigensystem. The perturbations can be numerical errors induced in discretization and computation. However, this situation does not affect the use of the modes because the numerical computed weak radiator modes, whose eigenvalues are nearly zero, are linear combinations of the modes without numerical approximations.

A numerical study was also performed for a uniform loading under concentrated masses attached at different locations to the spheroidal shell. The study showed the variations of

acoustic radiation due to alterations of structural components. The numerical results showed that the attached mass at the equatorial position induced more weakly radiating modes to be excited, but slightly changed the modal amplitudes of strongly radiating modes. This alteration in modal amplitudes results in the radiation pattern exhibiting more pressure in the direction of the symmetric axis of the spheroidal body. When masses were added at the apexes, the modal amplitudes produced are slightly different from those of the uniform thickness shell, of that the two radiation patterns are nearly identical.

ACKNOWLEDGMENT

The author would like to thank the National Science Council of the R.O.C. for financial support of this study under Contract NSC83-0209-E-019-026.

REFERENCES

1. P. T. Chen and J. H. Ginsberg 1995 *The Journal of the Acoustical Society of America* **98**, 3343–3351. Complex power, reciprocity, and radiation modes for submerged bodies.
2. G. V. Borgiotti 1990 *The Journal of the Acoustical Society of America* **88**, 1884–1893. The power radiated by a vibrating body in an acoustic fluid and its determination from boundary measurements.
3. D. M. Photiadis 1990 *The Journal of the Acoustical Society of America* **88**, 1152–1189. The relationship of singular value decomposition to wavevector filtering in sound radiation problems.
4. A. Sarkissian 1991 *The Journal of the Acoustical Society of America* **90**, 574–578. Acoustic radiation from finite structures.
5. K. A. Cunefare 1991 *The Journal of the Acoustical Society of America* **90**, 2521–2529. The minimum multimodal radiation efficiency of baffled finite beams.
6. K. Naghshineh and G. H. Koopmann 1992 *The Journal of the Acoustical Society of America* **92**, 841–855. Material tailoring of structures to achieve a minimum radiation condition.
7. K. A. Cunefare and G. H. Koopmann 1992 *Journal of Vibrations and Acoustics* **114**, 178–186. Acoustic design sensitivity for structural radiators.
8. K. Naghshineh and G. H. Koopmann 1993 *The Journal of the Acoustical Society of America* **93**, 2740–2752. Active control of sound power using acoustic basis functions as surface velocity filters.
9. K. Naghshineh and G. H. Koopmann 1992 *The Journal of the Acoustical Society of America* **92**, 856–870. A design method for achieving weak radiator structures using active vibration control.
10. P. T. Chen and J. H. Ginsberg 1993 *The Journal of the Acoustical Society of America* **94**, 221–233. Variational formulation of acoustic radiation from submerged spheroidal shells.
11. A. D. Pierce 1981 *Acoustics*, *An Introduction to Its Physical Principles and Applications*. New York: McGraw-Hill; chapter 3.
12. P. T. Chen and J. H. Ginsberg 1992 *The Journal of the Acoustical Society of America* **92**, 1499–1508. Modal properties and eigenvalue veering phenomena in axisymmetric vibration of spheroidal shells.
13. P. T. Chen and J. H. Ginsberg 1992 *Journal of Vibrations and Acoustics* **114**, 141–148. On the relationships between veering of eigenvalue loci and parameter sensitivity of eigenfunctions.